

# From Shelfbreak to Shoreline: Coastal Sea Level and Local Ocean Dynamics in the Northwest Atlantic

C. M. L. Camargo<sup>1</sup>, C. G. Piecuch<sup>1</sup>, B. Raubenheimer<sup>2</sup>

<sup>1</sup>Physical Oceanography Department, Woods Hole Oceanographic Institution, Woods Hole, United States

<sup>2</sup>Applied Ocean Physics and Engineering Department, Woods Hole Oceanographic Institution, Woods Hole, United States

## Key Points:

- Daily Shelfbreak Jet transports and Southern New England coastal sea levels are anti-correlated during 2014-2022.
- The observed relationship between these two variables is consistent with geostrophic balance.
- For this region, coastal sea levels are more sensitive to local ocean dynamics than to large-scale circulation.

---

Corresponding author: Carolina Camargo, [carolina.camargo@whoi.edu](mailto:carolina.camargo@whoi.edu)

## Abstract

Sea-level change threatens the U.S. East Coast. Thus, it is important to understand the underlying causes, including ocean dynamics. Most past studies emphasized links between coastal sea level and local atmospheric variability or large-scale circulation and climate, but possible relationships with local ocean currents over the shelf and slope remain largely unexplored. Here we use 7 years of in-situ velocity and sea-level data to quantify the relationship between northeastern U.S. coastal sea level and variable Shelfbreak Jet transport south of Nantucket Island. At timescales of 1–15 days, southern New England coastal sea level and transport vary in anti-phase, with magnitude-squared coherences of  $\sim 0.5$  and admittance amplitudes of  $\sim 0.3 \text{ m Sv}^{-1}$ . These results are consistent with a dominant geostrophic balance between along-shelf transport and coastal sea level, corroborating a hypothesis made decades ago that was not tested due to the lack of transport data.

## Plain Language Summary

Sea-level rise is an imminent threat to coastal communities worldwide including the U.S. East Coast. Therefore, it is crucial to understand the processes driving regional sea-level change. While past studies documented how coastal sea level may be influenced by large-scale ocean circulation, less attention has been paid to the role of more local currents over the shelf and slope. Here we explore the relationship between coastal sea level along the northeastern U.S. and the Shelfbreak Jet, a current that flows along the shelf-break from the Labrador Sea to Cape Hatteras (North Carolina). From 7 years of in-situ data of both current velocities and water levels, we see that as coastal sea level rises Shelfbreak Jet transport increases westward (and vice versa) on timescales of days to weeks. Our results lay the groundwork for understanding relationships between coastal sea level and local ocean dynamics elsewhere.

## 1 Introduction

Sea-level rise is one of the main threats to coastal communities worldwide. Understanding the causes of past coastal sea-level change is critical for constraining sea-level projections and better preparing for the impacts of climate change. In addition to global-mean sea level, coastal sea-level change is affected by spatially varying processes, such as the gravitational, rotational, and deformational effects of water mass redistribution, the inverted-barometer response to changes in air pressure, and ocean dynamics (Stammer et al., 2013). The link between coastal sea level and particular ocean-circulation features is still, in general, poorly understood.

Coastal sea level along northeastern North America has been the subject of many past papers (e.g., Piecuch, 2020, and references therein). Sea level in this region has been mainly related to aspects of large-scale ocean circulation and climate, including the North Atlantic Oscillation (Andres et al., 2013; Kenigson et al., 2018; McCarthy, Haigh, et al., 2015; Woodworth et al., 2017), El Niño-Southern Oscillation (Park & Dusek, 2013; Hamlington et al., 2015), the Atlantic meridional overturning circulation (AMOC, Goddard et al., 2015; Little et al., 2019; Piecuch et al., 2019; Yin et al., 2009; Yin & Goddard, 2013) and the Gulf Stream (Diabaté et al., 2021; Dong et al., 2019). South of Cape Hatteras, coastal sea-level variations have a strong anti-phase relationship with changes in the Gulf Stream transport, across a range of timescales and periods (Montgomery, 1938; Noble & Gelfenbaum, 1992; Park & Sweet, 2015; Stommel, 1958; Thompson, 1986). North of Cape Hatteras, along the Mid-Atlantic Bight and Gulf of Maine, a link between coastal sea level and large-scale open-ocean circulation is less clear. There, local processes over the shelf and slope may exert a stronger influence on sea level (e.g., Noble & Butman, 1979; Piecuch & Ponte, 2015; Sandstrom, 1980; Thompson, 1986; Woodworth et al., 2014). For instance, coastal sea-level variability along the Mid-Atlantic Bight and Gulf of Maine

64 has been related to local along-shore winds (Andres et al., 2013; Chen et al., 2020; Y. Li  
65 et al., 2014; Noble & Butman, 1979; Piecuch et al., 2016), changes in local barometric  
66 pressure (Piecuch & Ponte, 2015; Zhu et al., 2023), density anomalies originating in the  
67 subpolar gyre and Labrador Sea (Dangendorf et al., 2021; Frederikse et al., 2017; Mi-  
68 nobe et al., 2017) and river discharges (Piecuch et al., 2018). Other important drivers  
69 of sea-level variability in this region may include remote wind and buoyancy forcing (Wang  
70 et al., 2022, 2024). However, even models that incorporate all of these effects are unable  
71 to fully account for all of the variability present in sea-level observations (e.g., Wang et  
72 al., 2022), suggesting that there remains more for us to learn about the drivers of coastal  
73 sea level along northeastern North America. Additionally, there have been few attempts  
74 to directly relate northeastern North American coastal sea level and local ocean circu-  
75 lation, mainly due to the lack of available observations.

76 One of the most notable features in the Northwest Atlantic is the aforementioned  
77 Gulf Stream (Figure 1), a strong western boundary current that plays a role in both the  
78 AMOC and the wind-driven gyre circulation, carrying warm waters from the Florida Strait  
79 along the South Atlantic Bight until Cape Hatteras, North Carolina (Andres, 2021; Hei-  
80 derich & Todd, 2020; Rossby et al., 2014; Stommel, 1958). At Cape Hatteras, the Gulf  
81 Stream detaches from the coast and becomes a meandering free jet, flowing eastward into  
82 the open ocean, after which two recirculation cells are formed on either side: an anti-  
83 cyclonic cell south of the Gulf Stream over the Sargasso Sea; and a cyclonic cell north  
84 of the Gulf Stream over the Slope Sea (Andres et al., 2013, 2020; Csanady & Hamilton,  
85 1988). The latter gyre includes the Slope Current, a relatively strong feature offshore  
86 of the shelf (Flagg et al., 2006). Onshore of the slope current, roughly centered over the  
87 continental shelfbreak, is the Shelfbreak Jet (SBJ), which represents a boundary between  
88 fresher nearshore waters and saltier open-ocean waters, and carries cold waters from the  
89 Labrador Sea towards Cape Hatteras following the shelfbreak (Flagg et al., 2006; Forsyth  
90 et al., 2020; Fratantoni et al., 2001; Fratantoni & Pickart, 2003, 2007; Linder & Gawarkiewicz,  
91 1998). The shelfbreak region is also subject to Gulf Stream rings (Silver et al., 2021),  
92 which sometimes interact with the shallow bathymetry, interrupting the SBJ (Forsyth  
93 et al., 2022).

94 Nearly four decades ago, Thompson (1986) hypothesized that the time-variable depth-  
95 dependent dynamics of currents over the shelf and upper slope, such as the SBJ, might  
96 substantially influence coastal sea-level variability north of Cape Hatteras. This hypoth-  
97 esis, however, has remained largely unexplored due to the lack of observational data. Here  
98 we use unprecedentedly long (7-year) observational records of hourly velocity data from  
99 the Ocean Observatory Initiative (OOI) Coastal Pioneer Array, together with data from  
100 a dense network of coastal tide gauges, to test the hypothesis that coastal sea level is cou-  
101 pled to circulation over the shelf and slope. Our study focuses on characterizing the re-  
102 lationship between the SBJ and sea level along the northeastern United States, with par-  
103 ticular emphasis on Southern New England.

## 104 2 Material and Methods

### 105 2.1 Data

#### 106 2.1.1 Coastal sea level

107 We use data from 31 tide-gauge stations along the northeastern United States pro-  
108 vided by the NOAA tides and currents portal (Figure 2a, Table S1). Hourly water level  
109 (hereinafter sea level) and barometric pressure are downloaded for each station from 2014  
110 until 2023. We use the pressure data to remove the local inverted barometer contribu-  
111 tion from the tide-gauge sea-level measurements (Pugh & Woodworth, 2014). Given the  
112 large scales of barometric-pressure variability (Figure S1), for stations with incomplete  
113 barometric-pressure records, we filled data gaps with a regional average of contempo-

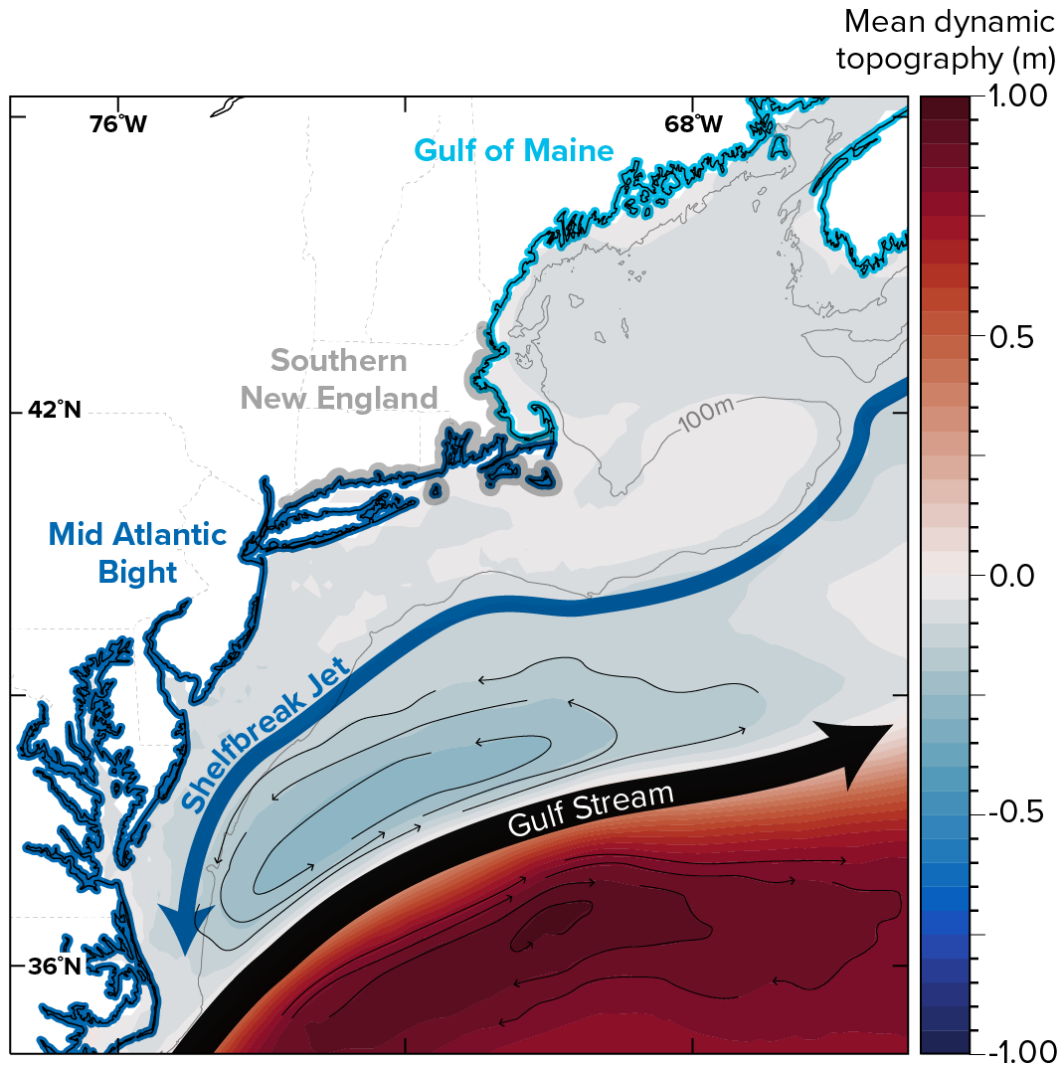


**Figure 1.** Oceanographic features of the northwestern North Atlantic Ocean. Colors indicate the mean dynamic topography in meters (Jousset, 2023). The mean position of the Gulf Stream and the Shelfbreak Jet are indicated by the black and blue arrows, respectively. The two recirculation cells over the Slope and Sargasso sea are delineated by highs and lows in the mean dynamic topography contour lines. Also indicated in the map is the Gulf of Maine (from Cape Code to Cape Sable Island, Nova Scotia), Mid Atlantic Bight, Southern New England, and the 100-m isobath (light gray line).

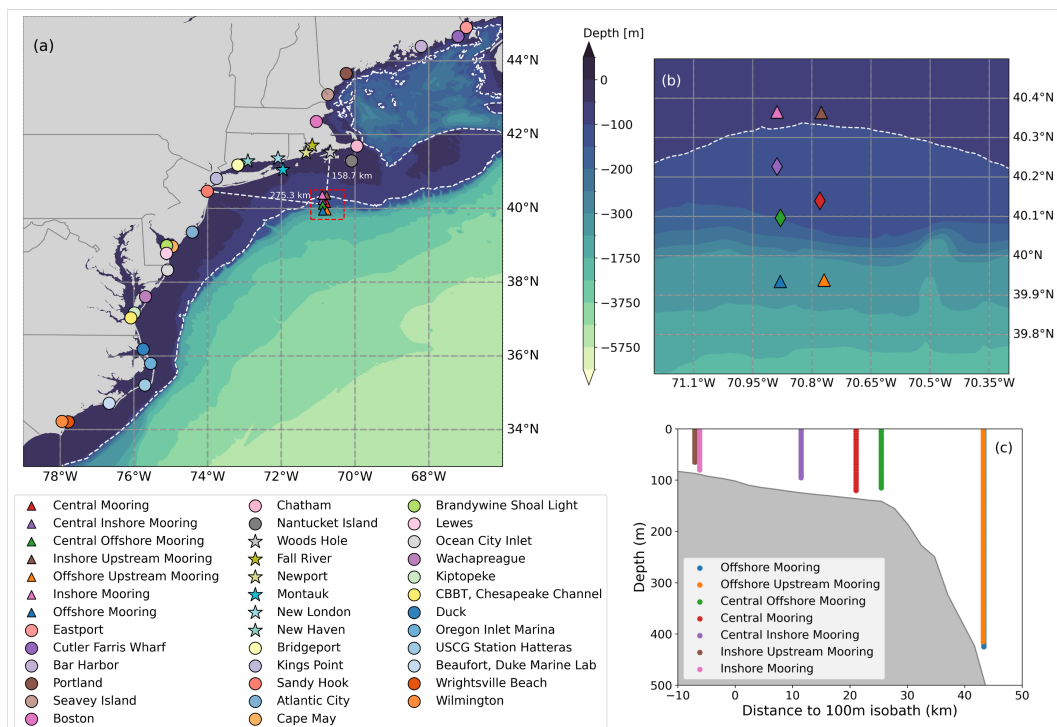


**Figure 2.** Map of the study area. (a) Regional map showing the locations of tide gauges (filled circles and stars, key at bottom) and of the Pioneer array (filled triangles and diamonds in dashed red box). (b) Zoom-in of the Pioneer array (see red box in a). (c) Depth versus cross-shelf distance of the Pioneer array moorings. Colored contours in (a) and (b) indicate bathymetry (from the General Bathymetric Chart of the Oceans, <https://www.gebco.net/>), and the white dashed line the 100-m isobath. Starred stations in (a) indicate the stations along the Southern New England coast, from which data are averaged in Figures 3 and 5.

114 raneous barometric-pressure from stations within a 200-km radius. Tides are removed  
 115 via harmonic analysis (Utide; Codiga, 2011). We use the 68 standard tidal constituents  
 116 estimated by Utide, except for the solar annual and semiannual astronomical tides, which  
 117 cannot be distinguished from the mean sea level seasonal cycle driven by wind stress and  
 118 buoyancy fluxes (e.g., Vinogradov et al., 2008). Other contributions to the sea level sig-  
 119 nal, such as land motion, mass redistribution and global mean sea-level, are assumed to  
 120 be negligible on the sub-seasonal timescales examined here.

### 121 **2.1.2 Shelfbreak Jet velocity and transport**

122 Jet transport is derived using velocity data from the OOI Coastal Pioneer Array  
 123 (Gawarkiewicz & Plueddemann, 2020). The Array is located at the New England shelf-  
 124 break, about 75 nautical miles ( $\sim 160$  km) south of Martha’s Vineyard (Figure 2a), and  
 125 comprises 7 oceanographic moorings spread from the shelf to offshore of the shelfbreak  
 126 (Figure 2b,c). The foot of the Shelfbreak Front typically lies between the inshore and  
 127 central moorings, while the frontal outcrop lies between the central and offshore moor-  
 128 ings (Gawarkiewicz & Plueddemann, 2020). Since we want to characterize the SBJ, we  
 129 use data from the three central moorings, located around the 130-m isobath (127-, 135-  
 130 , and 147-m water depths) and about 10 to 30 km offshore of the 100-m isobath. Fur-  
 131 ther details can be found in Gawarkiewicz and Plueddemann (2020).

132 Each mooring has several oceanographic instruments, including a bottom-mounted  
 133 upward-looking Teledyne RDI Workhorse Acoustic Doppler Current Profiler (ADCP),  
 134 which measures zonal  $u$  (along-shelf, positive east upstream) and meridional  $v$  (cross-  
 135 shelf, positive north onshore) velocities throughout the water column. These are 150-  
 136 kHz ADCPs, with a burst sampling configuration of 90 pings 2 seconds apart at the top  
 137 of each hour, that is an hourly sampling frequency of 0.5 Hz and 4-m vertical resolution.  
 138 Quality controlled data is downloaded from the OOI portal in Earth Coordinates (aligned  
 139 to geographic north). Although the processed data is provided at 30-minute intervals,  
 140 we average onto hourly intervals, which is the original temporal resolution, and which  
 141 is consistent with tide-gauge records. In addition, we grid all ADCP data onto a com-  
 142 mon vertical axis.

143 We apply 4 additional criteria to the data. First, we remove instances when less  
 144 than 80% of the pings within the burst were considered reliable for velocity measurement,  
 145 considering all 4 beams of the ADCP (Côté et al., 2011). We then remove data from the  
 146 top 10% of the water column, which is often contaminated by surface reflection, and ap-  
 147 ply a global range filter, removing any measurements with velocities larger than  $\pm 2 \text{ m s}^{-1}$ .  
 148 Finally, we remove any time steps with abrupt depth changes, removing erroneous mea-  
 149 surements when the ADCP was out of position or inclined.

150 To reduce the number of gaps in the data and tamp down errors, we compute the  
 151 regional average of the depth-dependent along-shelf SBJ velocities across the three cen-  
 152 tral moorings. This gives a temporally complete along-shore velocity time series, as a  
 153 function of depth, from April 2014 until November 2022. Since cross-shore velocity vari-  
 154 ations are relatively small and along-shore velocities from the individual central moor-  
 155 ings are all highly correlated with one another (average Pearson’s correlation of 0.8; Fig-  
 156 ure S2), this averaging process does not introduce appreciable errors. Similarly to the  
 157 tide gauges, we remove tides via a harmonic analysis (Utide, Codiga (2011)), using the  
 158 same 66 tidal constituents as before.

159 Jet transport  $Q$  is computed using the depth integral of the zonal velocity  $u$  as

$$Q = W \int_{115 \text{ m}}^{15 \text{ m}} u dz, \quad (1)$$

160 where  $W$  is a jet width scale. We integrate from 15 to 115 m to avoid the surface and  
 161 bottom layers where there is a lot of missing data. Summing over this depth range re-  
 162 turns an integrated velocity that is about 7% smaller than if we included the entire wa-  
 163 ter column. Based on previously reported SBJ transports, we estimate a representative  
 164 width value of 40 km, which is comparable to previously reported SBJ widths (Table S2;  
 165 Flagg et al., 2006; Forsyth et al., 2020; Linder & Gawarkiewicz, 1998).

## 166 2.2 Spectral analysis

167 To investigate the relationship between coastal sea level  $\eta(t)$  and SBJ transport  $Q(t)$ ,  
 168 where  $t$  is time, we first compute the magnitude-squared coherence  $C_{Q\eta}^2(f)$ , defined as

$$C_{Q\eta}^2(f) = \frac{|P_{Q\eta}(f)|^2}{P_{\eta\eta}P_{QQ}}, \quad (2)$$

169 where  $P_{\eta Q}(f)$  is the cross-spectral density between  $\eta(t)$  and  $Q(t)$  at frequency  $f$ , and  
 170  $P_{\eta\eta}(f)$  and  $P_{QQ}(f)$  are the respective power spectral densities (Bendat & Piersol, 2010;  
 171 Quinn & Ponte, 2012; Thomson & Emery, 2014; Vinogradova et al., 2007). The magnitude-  
 172 squared coherence is the frequency-domain analogue of squared correlation (coefficient  
 173 of determination) in the time domain. In addition, we compute the admittance (or trans-  
 174 fer function), which can be interpreted as a complex-valued regression coefficient com-  
 175 puted as a function frequency

$$A_{Q\eta}(f) = \frac{P_{Q\eta}(f)}{P_{QQ}(f)}. \quad (3)$$

176 Note that, while  $C_{Q\eta}^2(f)$  is dimensionless,  $A_{Q\eta}(f)$  has dimensions of sea level per trans-  
 177 port ( $\text{m Sv}^{-1}$ ). Coherence and admittance are computed with the Scipy package ([https://  
 178 scipy.org/](https://scipy.org/)). To increase the signal-to-noise ratio for the main timescales of interest (pe-  
 179 riods between 1 and 15 days), we average over 209 blocks of 360-hour-long segments with  
 180 a Flattop window and no overlap. Thus, we can resolve periods between 0.08 and 15 days.  
 181 Note that we tested other analysis choices (e.g., Hann window, 50% overlap), and the  
 182 results are qualitatively robust (not shown). Confidence level is computed based on Monte  
 183 Carlo simulation as the 95<sup>th</sup> percentile of repeated coherence analyses made on 1000 pairs  
 184 of random white-noise samples. This gives virtually the same value as textbook estimates  
 185 based on effective degrees of freedom (0.014, Thomson & Emery, 2014).

186 To explore the dependence of the coherence and admittance on time interval, we  
 187 perform wavelet transforms, which can be used to compute both wavelet (magnitude-  
 188 squared) coherence (Grinsted et al., 2004)

$$WTC_{Q\eta} = \frac{|W_n^{Q\eta}(s)|^2}{W_n^\eta(s)W_n^Q(s)}, \quad (4)$$

189 and admittance (Audet, 2011)

$$WTA_{Q\eta} = \frac{W_n^{Q\eta}(s)}{W_n^Q(s)}. \quad (5)$$

190 Here  $W_n^x(s)$  is the continuous wavelet transform of a single time series  $x$ ,  $W_n^{xy}(s)$  is the  
 191 cross-wavelet transform between two time series  $x$  and  $y$ ,  $n$  is dimensionless time, and  
 192  $(s)$  is the scale stretching time (Grinsted et al., 2004). The wavelet coherence and ad-  
 193 mittance can be thought of as localized frequency-domain analogues of squared correla-  
 194 tion and regression coefficient, respectively (Grinsted et al., 2004; Stark et al., 2003).  
 195 We use Grinsted et al. (2004)'s wavelet package, with a Morlet Wavelet and smoothing  
 196 of 1/12 scales per octave. Significance levels are based on repeated Monte Carlo simu-  
 197 lations with 1000 randomly generated time series.

### 198 3 Results

199 Daily sea level averaged along the Southern New England coast and SBJ transport  
 200 are anti-correlated over the 7-year study period (Figure 3a). Considering all timescales  
 201 in the data, we compute a Pearson correlation of  $-0.54$ , and a regression coefficient of  
 202  $-0.17 \text{ m Sv}^{-1}$  between the two records. Given the westward sense of SBJ flows, this in-  
 203 dicates that sea level tends to rise by 17 cm for a 1 Sv increase in SBJ transport, and  
 204 vice versa for a sea-level fall and SBJ-transport decrease. The relationship between coastal  
 205 sea level and SBJ transport is more clearly visualized in Figure 3b, which presents a zoom-  
 206 in on a shorter period. Note that the summers of 2014 and 2015 are exceptions to the  
 207 rule, when sea level and SBJ transport are uncorrelated, and some prominent transport  
 208 fluctuations are not mirrored in sea level (Figure S3). While both time series vary over  
 209 a range of timescales, both show a clear seasonality, particularly in terms of a seasonal  
 210 oscillation in the magnitudes of daily-to-weekly variability, with stronger variability over  
 211 the winter months. In fact, high-frequency variability explains a substantial portion of  
 212 the total data variance. For example, 66% and 43% of the daily sea-level and transport  
 213 variance, respectively, is explained by variability at periods between 1 and 15 days (Fig-  
 214 ure 3e,f). Indeed, isolating the 1–15-day band, we obtain stronger correlation (0.61) and  
 215 regression ( $-0.27 \text{ m Sv}^{-1}$ ) coefficients between sea level and SBJ transport (Figure 3e).  
 216 Therefore, we pay particular, but not exclusive, attention to high frequencies in what  
 217 follows.

218 Magnitude squared-coherence and admittance between SBJ transport and South-  
 219 ern New England coastal sea level vary substantially with frequency (Figure 3c). Coher-  
 220 ence hovers around zero for timescales shorter than the inertial period ( $\sim 19$  hours), but  
 221 values become larger at lower frequencies, for example, increasing from 0.25 at 1-day pe-

222 riod to 0.45 at 15-day period. Coherence peaks at 0.53 at 36-hour period, with corre-  
 223 sponding admittance magnitude of  $0.29 \text{ m Sv}^{-1}$ . Note that while the coherence is almost  
 224 always statistically significant (95% confidence level is 0.014), only higher coherence lev-  
 225 els should be interpreted as physically significant. For example, a coherence of 0.3 means  
 226 that for a certain frequency, one variable can explain 30% of the variance in the other  
 227 variable at that frequency. For periods between 2 and 4 days, the coherence decreases  
 228 to 0.36, while the admittance shows a small increase reaching 0.32. For periods longer  
 229 than 4 days, coherence reaches a plateau around 0.45, while the admittance decreases  
 230 to 0.25. The admittance phase reveals that both variables are anti-phased, with a phase  
 231 of 180 degrees for periods larger than 1 day (Figure 3d). These admittance and coher-  
 232 ence values are roughly consistent with the signs and magnitudes of the correlation and  
 233 regression coefficients given earlier. The anti-phase relationship between sea level and  
 234 SBJ transport at periods longer than  $\sim 1$  day is consistent with a general expectation  
 235 for a dominant geostrophic balance at timescales longer than inertial.

236 Coherence and admittance between SBJ transport and individual tide-gauge records  
 237 along the northeastern United States show a clear frequency-dependent spatial structure  
 238 (Figure 4). Peak coherence occurs first and with stronger magnitude at the stations closer  
 239 to the Array, along the Southern New England coast. Further from it, smaller peaks ap-  
 240 pear towards lower frequencies. At periods from 1 to 2 days, the stations from Woods  
 241 Hole to Kings Point show higher coherence, with admittances varying from 0.22 to  $0.39$   
 242  $\text{m Sv}^{-1}$ . However, geographic distance alone does not entirely explain the observed pat-  
 243 terns, since the Nantucket Island and Chatham stations, which are also relatively close  
 244 to Pioneer, show lower coherence for this period, indicating that other processes around  
 245 Nantucket are important for determining sea-level variations in these locations on these  
 246 timescales.

247 For periods between 2 to 4 days, the area of higher coherence ( $> 0.3$ ) extends down-  
 248 stream to Delaware Bay (Lewes). This is the range of periods with the strongest admit-  
 249 tance values, varying from 0.24 to  $0.41 \text{ m Sv}^{-1}$ . The 2–4-day period is comparable to  
 250 the time it would take a signal to propagate from the Pioneer Array to Delaware Bay  
 251 at a nominal Kelvin wave speed of  $2\text{--}3 \text{ m s}^{-1}$  (Hughes et al., 2019). For periods from  
 252 4 to 15 days, higher coherence extends even further afield, reaching from the Gulf of Maine  
 253 (Cutler Farris Wharf) down to North Carolina (Duck). We see no physically significant  
 254 coherence at any frequency downstream of Cape Hatteras (note that our analysis does  
 255 not include stations farther south than North Carolina). This suggests that the SBJ dy-  
 256 namics influence on sea level simply do not extend farther south or that other factors  
 257 are more important to sea-level variability in that region (e.g., coastal geometry, prox-  
 258 imity of the Gulf Stream to shore).

259 Wavelet coherence between Southern New England coastal sea level and SBJ trans-  
 260 port is generally intermittent and in anti-phase (Figure 5). That is, for some frequency  
 261 bands, sea level and SBJ transport are significantly coherent during some time intervals  
 262 but not others. These complex, granular patterns are smoothed out in the block-averaged  
 263 picture painted by the earlier coherence analysis (Figure 3). We see a strong seasonal  
 264 modulation of higher-frequency (1–46 day) coherence, which is weak and mostly insignif-  
 265 icant in the summer (June to August) and stronger and largely significant in winter (Novem-  
 266 ber to February). However, the admittance at 20–40-day periods is lower than at 1–15-  
 267 day period, suggesting that sea level is less sensitive to SBJ transports at these longer  
 268 periods. This is consistent with our earlier finding that correlation and regression coef-  
 269 ficients between sea level and SBJ transport are higher when we bandpass the data to  
 270 isolate variability at 1–15-day periods. Times when sea level and SBJ transport are co-  
 271 herent at periods between 10 to 30 days might also be connected to intrusion of warm  
 272 core rings onto the shelf, which have an average advective time scale of about 30 days,  
 273 and are known to disrupt the SBJ (Forsyth et al., 2022). Another noticeable feature is  
 274 the strong coherence in 2018 at 40–180-day period with duration of almost a full year.

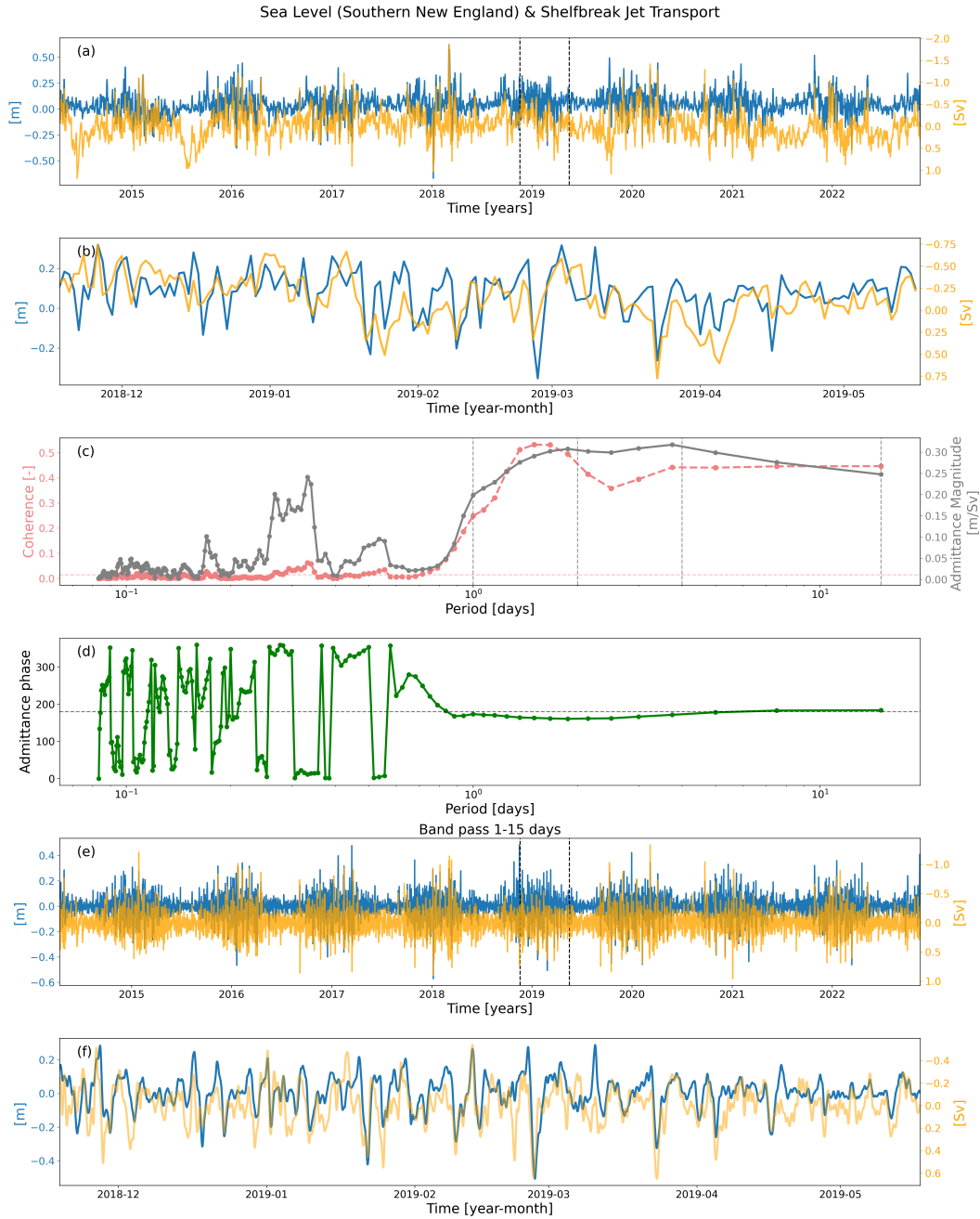


**Figure 3.** Time series of daily sea level along the Southern coast of New England (blue line, left axis, meters), and of Shelfbreak Jet (SBJ) transport (orange line, right axis, Sv) for the entire record (a) and for 180 days (b) during the period between the vertical dotted lines in (a). (c) Coherence (pink, left axis) and admittance magnitude (gray, right axis, in  $\text{m Sv}^{-1}$ ) between sea level and SBJ transport time series versus period. Horizontal dashed line indicates the 95% confidence level, and vertical lines indicate, from left to right, 1-, 2-, 4-, and 15-day periods. (d) Admittance phase (degrees) versus period. Hourly time series band-passed over 1–15 days for the entire record (e) and for the 180 days (f) delineated by the vertical dotted lines in (e). The right vertical axis in (a), (b), (f), and (e), regarding SBJ time series, is inverted, emphasizing that a negative SBJ anomaly is related to a positive sea-level anomaly.

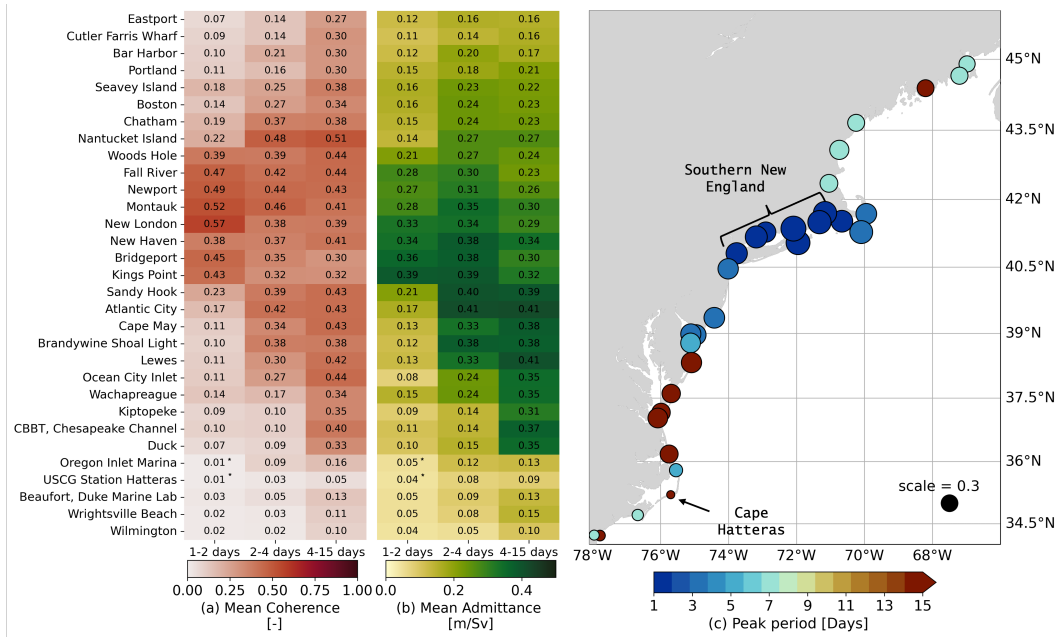


**Figure 4.** Mean magnitude-squared coherence (a, left) and admittance amplitude (b, middle) between Shelfbreak Jet transport and sea level at tide gauges ranging from Eastport, Maine (top row) down to Wrightville Beach, North Carolina (last row), averaged between 1 to 2 days (left column), 2 to 4 days (middle column) and 4 to 15 days (right columns), with the tide gauges ordered following the coastline from North to South. Asterisk indicates statistically insignificant values. Regional map (c, right) indicating the period (color) and magnitude (size) of maximum coherence. Key locations used for interpretation are indicated in the map.

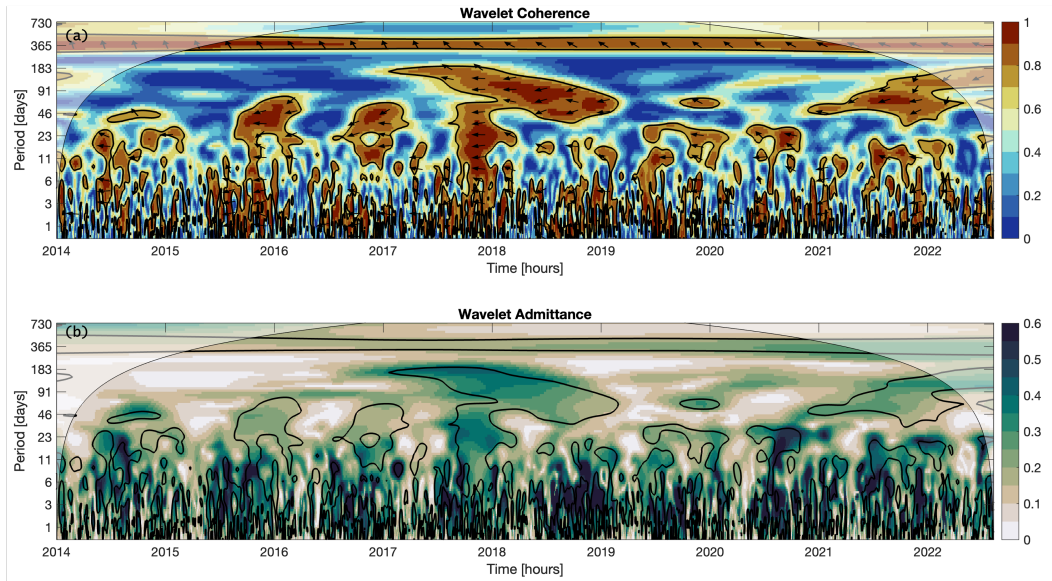


**Figure 5.** Wavelet coherence (a, top) and admittance (b, bottom) between sea level and Shelfbreak Jet transport. Vertical axis is the period in days, and admittance in  $\text{m Sv}^{-1}$ . Black contour lines indicate significant area at 95% confidence. Black arrows show the wavelet phase, with right and left arrows indicating in-phase and anti-phase, respectively, and up and down arrows indicating quadrature.

275 Finally, there is significant coherence during all time intervals at the annual period, but  
 276 admittance amplitudes are low and the phase indicates more of a quadrature relation-  
 277 ship, which is inconsistent with a dominant geostrophic balance.

#### 278 4 Discussion

279 In this work we characterized the relationship between coastal sea level along the  
 280 Northwest Atlantic and the SBJ transport based on observations. We found that coastal  
 281 sea level along Southern New England is significantly coherent with SBJ transport at  
 282 1–15-day periods, with coherence between the signals extending farther along the coast  
 283 for the longer periods. This unique analysis of multi-year records of local circulation and  
 284 coastal sea level allowed us to corroborate a hypothesis made decades ago that had never  
 285 been tested. Our findings provide valuable insight and complement past studies by shed-  
 286 ding light on processes contributing to sea-level changes that were previously overlooked,  
 287 serving as a reference point for understanding similar phenomena in different regions.

288 Our results are roughly consistent with expectations from ocean dynamics. Bingham  
 289 and Hughes (2009) made a thermal-wind argument that the sensitivity of coastal sea level  
 290 to alongshore upper-ocean transport is  $-2f/gH$ , where  $f$  is the Coriolis parameter,  $g$   
 291 is gravity, and  $H$  is the thickness of the upper ocean layer. Using  $H = 80$  m based on  
 292 the mean grounding position of the SBJ, we obtain a sensitivity of  $-0.25 \text{ m Sv}^{-1}$ , which  
 293 roughly agrees in sign and order of magnitude with our results (Figure 3). Note that this  
 294 crude estimate ignores important details of bathymetric variation. In contrast, the sensi-  
 295 tivity of coastal sea level to a variation in AMOC transport is approximately  $-0.02 \text{ m Sv}^{-1}$   
 296 (Little et al., 2019, and references therein), an order of magnitude smaller than with the  
 297 SBJ. That is, Southern New England sea level is more sensitive to variations in SBJ trans-  
 298 port than to equal transport variations in the AMOC. However, SBJ transport fluctu-

299 ations are about an order of magnitude or so smaller than AMOC transport variations  
300 (Forsyth et al., 2020; McCarthy, Smeed, et al., 2015). Thus, the respective dynamics of  
301 the SBJ and AMOC may have comparable influences on coastal sea level.

302 Geostrophic balance is a diagnostic relationship, not a statement of cause and ef-  
303 fect. Thus, our results do not suggest that transport changes drive sea-level changes (or  
304 vice versa), but rather suggest that common drivers induce variations in both SBJ and  
305 coastal sea level. For example, local wind forcing might explain the tandem fluctuations  
306 of sea level and the jet transport, as discussed in previous studies (e.g., Noble & But-  
307 man, 1979; Noble & Gelfenbaum, 1992; Sandstrom, 1980). The observed covariance be-  
308 tween SBJ transport and coastal sea level may also be tied to instabilities of the shelf-  
309 break front or the Gulf Stream. For example, the average instability (meandering) time  
310 scale of the SBJ ranges from about 4 to 15 days (Fratantoni & Pickart, 2003; Garvine  
311 et al., 1988; Gawarkiewicz, 1991; Gawarkiewicz et al., 2004; Lozier et al., 2002). Thus,  
312 the high coherence on the 1–15-day band could be linked to the meandering time scale  
313 of the SBJ. Likewise, influences of Gulf-Stream rings and instabilities interacting with  
314 the bathymetry of the continental margin may also be relevant (e.g., Cherian & Brink,  
315 2016, 2018). Furthermore, the spatial pattern of significant coherence might be related  
316 to the coastline geometry, or to the influence of winds in the region, which strengthen  
317 the SBJ between Nantucket and Long Island Sound (Lobert et al., 2023). For example,  
318 south of the Hudson Canyon (New Jersey), the dominant wind direction changes, which  
319 could explain why coherence between 1–2 days is lower in this region. Future studies should  
320 interrogate the forcing and dynamics mediating the relationship between the SBJ and  
321 sea level, which is important to understand to what extent coarse-resolution climate mod-  
322 els, that do not resolve the SBJ, accurately simulate coastal sea level.

323 We demonstrated that SBJ transport and sea level are coherent across a range of  
324 timescales. This implies that changes in one variable are partly informative of changes  
325 in the other. Since only short records of SBJ transport exist, one might use the longer  
326 tide-gauge time series, which are available for some locations going back more than a cen-  
327 tury, to reconstruct some aspects of past SBJ variability. While the amount of variabil-  
328 ity we can reconstruct may be limited, future studies could also incorporate other vari-  
329 ables relevant to the SBJ, such as temperature and salinity. Such an effort may, if suc-  
330 cessful, be informative for determining whether contemporary coastal ocean changes are  
331 anomalous in a wider historical context (e.g., Piecuch, 2020, and references therein).

332 Our results also have implications for coastal flooding studies. The frequency of  
333 high-tide flooding is rapidly increasing along the U.S. coasts (Moftakhari et al., 2015),  
334 making it important that we understand all the factors that contribute to such events.  
335 Customarily, the different components affecting coastal water levels are identified largely  
336 through harmonic analysis and filtering techniques, which enables the effects of mean  
337 sea-level changes to be distinguished from astronomical tides and storm surges (e.g., Sun  
338 et al., 2023; S. Li et al., 2022). Here, however, we illustrated that SBJ-related variabil-  
339 ity is relevant at timescales of 1 to 15 days, which roughly coincides with the storm surge  
340 frequency band. Thus, it is important to determine to what extent SBJ dynamics are  
341 interwoven with more familiar storm-surge processes related to winds, waves, and pres-  
342 sure, and to what extent SBJ processes play a role in high-tide flooding.

343 In addition to SBJ transport, sea level may also be sensitive to other aspects of SBJ  
344 variability, such as meandering, broadening or narrowing of the jet and cross-shore move-  
345 ment (Wise et al., 2018). However, the fixed position of the moorings does not allow an  
346 exploration of all these variables. Future studies using higher spatial resolution datasets,  
347 such as ocean models and satellite products, could investigate how coastal sea level re-  
348 sponds to variations in jet position and width. More generally, our study demonstrates  
349 the value of sustained, continuous coastal ocean observing of the shelf and slope for un-  
350 derstanding the dynamics of coastal sea-level variability.

351 **Open Research Section**

352 Tide gauge data is available at [https://tidesandcurrents.noaa.gov/stations](https://tidesandcurrents.noaa.gov/stations.html?type=Water+Levels)  
353 [.html?type=Water+Levels](https://tidesandcurrents.noaa.gov/stations.html?type=Water+Levels) (last accessed March/2024), and specific tide gauges names  
354 in Table S1. Pioneer Array data at the OOI Portal ([https://ooinet.oceanobservatories](https://ooinet.oceanobservatories.org/)  
355 [.org/](https://ooinet.oceanobservatories.org/), last accessed March/2024). Specific links to central moorings ADCPs are: [https://](https://ooinet.oceanobservatories.org/data_access/?search=CP02PMCI-RII01-02-ADCPTG010)  
356 [ooinet.oceanobservatories.org/data\\_access/?search=CP02PMCI-RII01-02-ADCPTG010](https://ooinet.oceanobservatories.org/data_access/?search=CP02PMCI-RII01-02-ADCPTG010)  
357 (Central Inshore Profiler Mooring); [https://ooinet.oceanobservatories.org/data](https://ooinet.oceanobservatories.org/data_access/?search=CP02PMCO-RII01-02-ADCPTG010)  
358 [\\_access/?search=CP02PMCO-RII01-02-ADCPTG010](https://ooinet.oceanobservatories.org/data_access/?search=CP02PMCO-RII01-02-ADCPTG010) (Central Offshore Profiler Mooring);  
359 [https://ooinet.oceanobservatories.org/data\\_access/?search=CP01CNSM-MFD35](https://ooinet.oceanobservatories.org/data_access/?search=CP01CNSM-MFD35-01-ADCPTF000)  
360 [-01-ADCPTF000](https://ooinet.oceanobservatories.org/data_access/?search=CP01CNSM-MFD35-01-ADCPTF000) (Central Surface Mooring). The quality controlled Shelfbreak Jet trans-  
361 port time series is available at <https://doi.org/10.5281/zenodo.10814048> (Camargo,  
362 2024).

363 **Acknowledgments**

364 C.M.L.C. was supported by funds from the Francis E. Fowler IV Center for Ocean and  
365 Climate at Woods Hole Oceanographic Institution. C.G.P. was supported by the NASA  
366 Sea Level Change Team (grant 80NSSC20K1241), Ocean Surface Topography Science  
367 Team (Jet Propulsion Laboratory Subcontract 1670515), and the National Science Founda-  
368 tion (award OCE-2123692). B.R. was supported by the National Science Foundation  
369 (award OCE-1848650). Figure 1 was produced by Natalie Renier (WHOI Creative Stu-  
370 dio). This material is based upon work supported by the Ocean Observatories Initiative  
371 (OOI), a major facility fully funded by the National Science Foundation under Coop-  
372 erative Agreement No. 1743430, and the Woods Hole Oceanographic Institution OOI  
373 Program Office.

374

**References**

375

Andres, M. (2021, September). Spatial and Temporal Variability of the Gulf Stream Near Cape Hatteras. *Journal of Geophysical Research: Oceans*, *126*(9), e2021JC017579. doi: 10.1029/2021JC017579

376

377

378

Andres, M., Donohue, K. A., & Toole, J. M. (2020, February). The Gulf Stream's path and time-averaged velocity structure and transport at 68.5°W and 70.3°W. *Deep Sea Research Part I: Oceanographic Research Papers*, *156*, 103179. doi: 10.1016/j.dsr.2019.103179

379

380

381

Andres, M., Gawarkiewicz, G. G., & Toole, J. M. (2013, November). Interannual sea level variability in the western North Atlantic: Regional forcing and remote response. *Geophysical Research Letters*, *40*(22), 5915–5919. doi: 10.1002/2013GL058013

382

383

384

385

Audet, P. (2011, January). Directional wavelet analysis on the sphere: Application to gravity and topography of the terrestrial planets. *Journal of Geophysical Research*, *116*(E1), E01003. doi: 10.1029/2010JE003710

386

387

388

Bendat, J. S., & Piersol, A. G. (2010). *Random Data: Analysis and Measurement Procedures* (1st ed.). Wiley. doi: 10.1002/9781118032428

389

390

391

Bingham, R. J., & Hughes, C. W. (2009, January). Signature of the Atlantic meridional overturning circulation in sea level along the east coast of North America. *Geophysical Research Letters*, *36*(2), 2008GL036215. doi: 10.1029/2008GL036215

392

393

394

Camargo, C. M. L. (2024, March). *Shelfbreak jet transport from OOI pioneer*. Zenodo. doi: 10.5281/zenodo.10814048

395

396

Chen, N., Han, G., & Yan, X.-H. (2020). Similarity and Difference in Interannual Sea Level Variations Between the Mid-Atlantic Bight and the Nova Scotia Coast. *Journal of Geophysical Research: Oceans*, *125*(5), e2019JC015919. doi: 10.1029/2019JC015919

397

398

399

400

Cherian, D. A., & Brink, K. H. (2016, December). Offshore Transport of Shelf Water by Deep-Ocean Eddies. *Journal of Physical Oceanography*, *46*(12), 3599–3621. doi: 10.1175/JPO-D-16-0085.1

401

402

403

Cherian, D. A., & Brink, K. H. (2018, May). Shelf Flows Forced by Deep-Ocean Anticyclonic Eddies at the Shelf Break. *Journal of Physical Oceanography*, *48*(5), 1117–1138. doi: 10.1175/JPO-D-17-0237.1

404

405

406

Codiga, D. L. (2011). *Unified Tidal Analysis and Prediction Using the UTide Matlab Functions* (Tech. Rep. No. GSO Technical Report 2011-01). Narragansett, RI: Graduate School of Oceanography, University of Rhode Island.

407

408

409

Côté, J. M., Hotchkiss, F. S., Martini, M., & Denham, C. R. (2011). *Acoustic Doppler Current Profiler (ADCP) Data Processing System Manual* (Tech. Rep. Nos. 00–458). Reston, Virginia: U.S. Geological Survey.

410

411

412

Csanady, G., & Hamilton, P. (1988, May). Circulation of slopewater. *Continental Shelf Research*, *8*(5-7), 565–624. doi: 10.1016/0278-4343(88)90068-4

413

414

415

Dangendorf, S., Frederikse, T., Chafik, L., Klinck, J. M., Ezer, T., & Hamlington, B. D. (2021, June). Data-driven reconstruction reveals large-scale ocean circulation control on coastal sea level. *Nature Climate Change*, *11*(6), 514–520. doi: 10.1038/s41558-021-01046-1

416

417

418

Diabaté, S. T., Swingedouw, D., Hirschi, J. J.-M., Duchez, A., Leadbitter, P. J., Haigh, I. D., & McCarthy, G. D. (2021, April). Western boundary circulation and coastal sea-level variability in northern hemisphere oceans. *Ocean Science*, *17*, 1449–1417. doi: 10.5194/os-17-1449-2021

419

420

421

422

Dong, S., Baringer, M. O., & Goni, G. J. (2019, April). Slow Down of the Gulf Stream during 1993–2016. *Scientific Reports*, *9*(1), 6672. doi: 10.1038/s41598-019-42820-8

423

424

425

Flagg, C. N., Dunn, M., Wang, D.-P., Rossby, H. T., & Benway, R. L. (2006, June). A study of the currents of the outer shelf and upper slope from a decade of shipboard ADCP observations in the Middle Atlantic Bight.

426

427

428

- 429 *Journal of Geophysical Research: Oceans*, 111(C6), 2005JC003116. doi:  
430 10.1029/2005JC003116
- 431 Forsyth, J., Andres, M., & Gawarkiewicz, G. (2020, September). Shelfbreak Jet  
432 Structure and Variability off New Jersey Using Ship of Opportunity Data  
433 From the *CMV Oleander*. *Journal of Geophysical Research: Oceans*, 125(9),  
434 e2020JC016455. doi: 10.1029/2020JC016455
- 435 Forsyth, J., Gawarkiewicz, G., & Andres, M. (2022, March). The Impact of Warm  
436 Core Rings on Middle Atlantic Bight Shelf Temperature and Shelf Break Ve-  
437 locity. *Journal of Geophysical Research: Oceans*, 127(3), e2021JC017759. doi:  
438 10.1029/2021JC017759
- 439 Fratantoni, P. S., & Pickart, R. S. (2003, May). Variability of the shelf break  
440 jet in the Middle Atlantic Bight: Internally or externally forced? *Jour-  
441 nal of Geophysical Research: Oceans*, 108(C5), 2002JC001326. doi:  
442 10.1029/2002JC001326
- 443 Fratantoni, P. S., & Pickart, R. S. (2007, October). The Western North Atlantic  
444 Shelfbreak Current System in Summer. *Journal of Physical Oceanography*,  
445 37(10), 2509–2533. doi: 10.1175/JPO3123.1
- 446 Fratantoni, P. S., Pickart, R. S., Torres, D. J., & Scotti, A. (2001, August). Mean  
447 Structure and Dynamics of the Shelfbreak Jet in the Middle Atlantic Bight  
448 during Fall and Winter\*. *Journal of Physical Oceanography*, 31(8), 2135–2156.  
449 doi: 10.1175/1520-0485(2001)031<2135:MSADOT>2.0.CO;2
- 450 Frederikse, T., Simon, K., Katsman, C. A., & Riva, R. (2017, July). The sea-level  
451 budget along the Northwest Atlantic coast: GIA, mass changes, and large-  
452 scale ocean dynamics. *Journal of Geophysical Research: Oceans*, 122(7),  
453 5486–5501. doi: 10.1002/2017JC012699
- 454 Garvine, R. W., Wong, K.-C., Gawarkiewicz, G. G., McCarthy, R. K., Houghton,  
455 R. W., & Aikman, F. (1988, December). The morphology of shelfbreak ed-  
456 dies. *Journal of Geophysical Research: Oceans*, 93(C12), 15593–15607. doi:  
457 10.1029/JC093iC12p15593
- 458 Gawarkiewicz, G. (1991, April). Linear Stability Models of Shelfbreak Fronts. *Jour-  
459 nal of Physical Oceanography*, 21.
- 460 Gawarkiewicz, G., Brink, K. H., Bahr, F., Beardsley, R. C., Caruso, M., Lynch,  
461 J. F., & Chiu, C.-S. (2004, March). A large-amplitude meander of the shelf-  
462 break front during summer south of New England: Observations from the  
463 Shelfbreak PRIMER experiment. *Journal of Geophysical Research: Oceans*,  
464 109(C3), 2002JC001468. doi: 10.1029/2002JC001468
- 465 Gawarkiewicz, G., & Plueddemann, A. J. (2020, January). Scientific rationale  
466 and conceptual design of a process-oriented shelfbreak observatory: The OOI  
467 Pioneer Array. *Journal of Operational Oceanography*, 13(1), 19–36. doi:  
468 10.1080/1755876X.2019.1679609
- 469 Goddard, P. B., Yin, J., Griffies, S. M., & Zhang, S. (2015, February). An ex-  
470 treme event of sea-level rise along the Northeast coast of North America in  
471 2009–2010. *Nature Communications*, 6(1), 6346. doi: 10.1038/ncomms7346
- 472 Grinsted, A., Moore, J. C., & Jevrejeva, S. (2004, November). Applica-  
473 tion of the cross wavelet transform and wavelet coherence to geophysical  
474 time series. *Nonlinear Processes in Geophysics*, 11(5/6), 561–566. doi:  
475 10.5194/npg-11-561-2004
- 476 Hamlington, B. D., Leben, R. R., Kim, K.-Y., Nerem, R. S., Atkinson, L. P., &  
477 Thompson, P. R. (2015). The effect of the El Niño-Southern Oscillation on  
478 U.S. regional and coastal sea level. *Journal of Geophysical Research: Oceans*,  
479 120(6), 3970–3986. doi: 10.1002/2014JC010602
- 480 Heiderich, J., & Todd, R. E. (2020, August). Along-Stream Evolution of Gulf  
481 Stream Volume Transport. *Journal of Physical Oceanography*, 50(8), 2251–  
482 2270. doi: 10.1175/JPO-D-19-0303.1
- 483 Hughes, C. W., Fukumori, I., Griffies, S. M., Huthnance, J. M., Minobe, S., Spence,

- 484 P., ... Wise, A. (2019, November). Sea Level and the Role of Coastal Trapped  
 485 Waves in Mediating the Influence of the Open Ocean on the Coast. *Surveys in*  
 486 *Geophysics*, 40(6), 1467–1492. doi: 10.1007/s10712-019-09535-x
- 487 Jousset, S. (2023). *Mean Dynamic Topography MDT CNES\_CLS 2022*. CNES. doi:  
 488 10.24400/527896/A01-2023.003
- 489 Kenigson, J. S., Han, W., Rajagopalan, B., Yanto, & Jasinski, M. (2018, July).  
 490 Decadal Shift of NAO-Linked Interannual Sea Level Variability along the  
 491 U.S. Northeast Coast. *Journal of Climate*, 31(13), 4981–4989. doi:  
 492 10.1175/JCLI-D-17-0403.1
- 493 Li, S., Wahl, T., Barroso, A., Coats, S., Dangendorf, S., Piecuch, C., ... Liu, L.  
 494 (2022). Contributions of Different Sea-Level Processes to High-Tide Flooding  
 495 Along the U.S. Coastline. *Journal of Geophysical Research: Oceans*, 127(7),  
 496 e2021JC018276. doi: 10.1029/2021JC018276
- 497 Li, Y., Ji, R., Fratantoni, P. S., Chen, C., Hare, J. A., Davis, C. S., & Beardsley,  
 498 R. C. (2014). Wind-induced interannual variability of sea level slope, along-  
 499 shelf flow, and surface salinity on the Northwest Atlantic shelf. *Journal of Geo-*  
 500 *physical Research: Oceans*, 119(4), 2462–2479. doi: 10.1002/2013JC009385
- 501 Linder, C. A., & Gawarkiewicz, G. (1998, August). A climatology of the shelfbreak  
 502 front in the Middle Atlantic Bight. *Journal of Geophysical Research: Oceans*,  
 503 103(C9), 18405–18423. doi: 10.1029/98JC01438
- 504 Little, C. M., Hu, A., Hughes, C. W., McCarthy, G. D., Piecuch, C. G., Ponte,  
 505 R. M., & Thomas, M. D. (2019, September). The Relationship Between U.S.  
 506 East Coast Sea Level and the Atlantic Meridional Overturning Circulation: A  
 507 Review. *Journal of Geophysical Research: Oceans*, 124(9), 6435–6458. doi:  
 508 10.1029/2019JC015152
- 509 Lobert, L., Gawarkiewicz, G., & Plueddemann, A. (2023, July). Categorization  
 510 of High-Wind Events and Their Contribution to the Seasonal Breakdown of  
 511 Stratification on the Southern New England Shelf. *Journal of Geophysical*  
 512 *Research: Oceans*, 128(7), e2022JC019625. doi: 10.1029/2022JC019625
- 513 Lozier, M. S., Reed, M. S. C., & Gawarkiewicz, G. G. (2002, March). Instability of  
 514 a Shelfbreak Front. *Journal of Physical Oceanography*, 32(3), 924–944. doi: 10  
 515 .1175/1520-0485(2002)032<0924:IOASF>2.0.CO;2
- 516 McCarthy, G. D., Haigh, I. D., Hirschi, J. J.-M., Grist, J. P., & Smeed, D. A. (2015,  
 517 May). Ocean impact on decadal Atlantic climate variability revealed by sea-  
 518 level observations. *Nature*, 521(7553), 508–510. doi: 10.1038/nature14491
- 519 McCarthy, G. D., Smeed, D. A., Johns, W. E., Frajka-Williams, E., Moat, B. I.,  
 520 Rayner, D., ... Bryden, H. L. (2015, January). Measuring the Atlantic  
 521 Meridional Overturning Circulation at 26°N. *Progress in Oceanography*, 130,  
 522 91–111. doi: 10.1016/j.pocean.2014.10.006
- 523 Minobe, S., Terada, M., Qiu, B., & Schneider, N. (2017, May). Western  
 524 Boundary Sea Level: A Theory, Rule of Thumb, and Application to Cli-  
 525 mate Models. *Journal of Physical Oceanography*, 47(5), 957–977. doi:  
 526 10.1175/JPO-D-16-0144.1
- 527 Moftakhari, H. R., AghaKouchak, A., Sanders, B. F., Feldman, D. L., Sweet, W.,  
 528 Matthew, R. A., & Luke, A. (2015). Increased nuisance flooding along the  
 529 coasts of the United States due to sea level rise: Past and future. *Geophysical*  
 530 *Research Letters*, 42(22), 9846–9852. doi: 10.1002/2015GL066072
- 531 Montgomery, R. (1938, January). Fluctuations in monthly sea level on eastern U.S.  
 532 coast as related to dynamics of western North Atlantic Ocean. *Journal of Ma-*  
 533 *rine Research*, 1(2).
- 534 Noble, M. A., & Butman, B. (1979). Low-frequency wind-induced sea level oscilla-  
 535 tions along the east coast of North America. *Journal of Geophysical Research:*  
 536 *Oceans*, 84(C6), 3227–3236. doi: 10.1029/JC084iC06p03227
- 537 Noble, M. A., & Gelfenbaum, G. R. (1992). Seasonal fluctuations in sea level on  
 538 the South Carolina shelf and their relationship to the Gulf Stream. *Journal of*

- 539 *Geophysical Research: Oceans*, 97(C6), 9521–9529. doi: 10.1029/92JC00811
- 540 Park, J., & Dusek, G. (2013, June). ENSO components of the Atlantic multidecadal  
541 oscillation and their relation to North Atlantic interannual coastal sea level  
542 anomalies. *Ocean Science*, 9(3), 535–543. doi: 10.5194/os-9-535-2013
- 543 Park, J., & Sweet, W. (2015, July). Accelerated sea level rise and Florida Current  
544 transport. *Ocean Science*, 11(4), 607–615. doi: 10.5194/os-11-607-2015
- 545 Piecuch, C. G. (2020). Drivers of US East Coast sea-level variability from years  
546 to decades in a changing ocean— What do we know and what do we need to  
547 know? *US Clivar Variations*, 18(3).
- 548 Piecuch, C. G., Bittermann, K., Kemp, A. C., Ponte, R. M., Little, C. M., Engel-  
549 hart, S. E., & Lentz, S. J. (2018, July). River-discharge effects on United  
550 States Atlantic and Gulf coast sea-level changes. *Proceedings of the National  
551 Academy of Sciences*, 115(30), 7729–7734. doi: 10.1073/pnas.1805428115
- 552 Piecuch, C. G., Dangendorf, S., Gawarkiewicz, G. G., Little, C. M., Ponte, R. M., &  
553 Yang, J. (2019, May). How is New England Coastal Sea Level Related to the  
554 Atlantic Meridional Overturning Circulation at 26° N? *Geophysical Research  
555 Letters*, 46(10), 5351–5360. doi: 10.1029/2019GL083073
- 556 Piecuch, C. G., Dangendorf, S., Ponte, R. M., & Marcos, M. (2016, July). Annual  
557 Sea Level Changes on the North American Northeast Coast: Influence of Local  
558 Winds and Barotropic Motions. *Journal of Climate*, 29(13), 4801–4816. doi:  
559 10.1175/JCLI-D-16-0048.1
- 560 Piecuch, C. G., & Ponte, R. M. (2015, July). Inverted barometer contributions to re-  
561 cent sea level changes along the northeast coast of North America. *Geophysical  
562 Research Letters*, 42(14), 5918–5925. doi: 10.1002/2015GL064580
- 563 Pugh, D., & Woodworth, P. (2014). *Sea-Level Science: Understanding Tides, Surges,  
564 Tsunamis and Mean Sea-Level Changes*. Cambridge: Cambridge University  
565 Press. doi: 10.1017/CBO9781139235778
- 566 Quinn, K. J., & Ponte, R. M. (2012, April). High frequency barotropic ocean vari-  
567 ability observed by GRACE and satellite altimetry. *Geophysical Research Let-  
568 ters*, 39(7), 2012GL051301. doi: 10.1029/2012GL051301
- 569 Rossby, T., Flagg, C. N., Donohue, K., Sanchez-Franks, A., & Lillibridge, J. (2014,  
570 January). On the long-term stability of Gulf Stream transport based on 20  
571 years of direct measurements. *Geophysical Research Letters*, 41(1), 114–120.  
572 doi: 10.1002/2013GL058636
- 573 Sandstrom, H. (1980, January). On the wind-induced sea level changes on the Sco-  
574 tian shelf. *Journal of Geophysical Research: Oceans*, 85(C1), 461–468. doi: 10  
575 .1029/JC085iC01p00461
- 576 Silver, A., Gangopadhyay, A., Gawarkiewicz, G., Silva, E. N. S., & Clark, J. (2021,  
577 January). Interannual and seasonal asymmetries in Gulf Stream Ring Forma-  
578 tions from 1980 to 2019. *Scientific Reports*, 11(1), 2207. doi: 10.1038/s41598  
579 -021-81827-y
- 580 Stammer, D., Cazenave, A., Ponte, R. M., & Tamisiea, M. E. (2013, January).  
581 Causes for Contemporary Regional Sea Level Changes. *Annual Review of  
582 Marine Science*, 5(1), 21–46. doi: 10.1146/annurev-marine-121211-172406
- 583 Stark, C. P., Stewart, J., & Ebinger, C. J. (2003, December). Wavelet transform  
584 mapping of effective elastic thickness and plate loading: Validation using  
585 synthetic data and application to the study of southern African tectonics.  
586 *Journal of Geophysical Research: Solid Earth*, 108(B12), 2001JB000609. doi:  
587 10.1029/2001JB000609
- 588 Stommel, H. (1958). *The Gulf Stream: A Physical and Dynamical Description*.  
589 Berkeley, Los Angeles and London: University of California Press and Cam-  
590 bridge University Press.
- 591 Sun, Q., Dangendorf, S., Wahl, T., & Thompson, P. R. (2023, December). Causes of  
592 accelerated High-Tide Flooding in the U.S. since 1950. *npj Climate and Atmo-  
593 spheric Science*, 6(1), 210. doi: 10.1038/s41612-023-00538-5

- 594 Thompson, K. R. (1986, October). North Atlantic sea-level and circula-  
 595 tion. *Geophysical Journal International*, *87*(1), 15–32. doi: 10.1111/  
 596 j.1365-246X.1986.tb04543.x
- 597 Thomson, R. E., & Emery, W. J. (2014). Data Analysis Methods in Physical  
 598 Oceanography. In *Data Analysis Methods in Physical Oceanography* (Third ed.,  
 599 p. iii). Elsevier. doi: 10.1016/B978-0-12-387782-6.01001-2
- 600 Vinogradov, S. V., Ponte, R. M., Heimbach, P., & Wunsch, C. (2008). The mean  
 601 seasonal cycle in sea level estimated from a data-constrained general cir-  
 602 culation model. *Journal of Geophysical Research: Oceans*, *113*(C3). doi:  
 603 10.1029/2007JC004496
- 604 Vinogradova, N. T., Ponte, R. M., & Stammer, D. (2007, February). Rela-  
 605 tion between sea level and bottom pressure and the vertical dependence of  
 606 oceanic variability. *Geophysical Research Letters*, *34*(3), 2006GL028588. doi:  
 607 10.1029/2006GL028588
- 608 Wang, O., Lee, T., Frederikse, T., Ponte, R. M., Fenty, I., Fukumori, I., & Hamling-  
 609 ton, B. D. (2024, January). What Forcing Mechanisms Affect the Interan-  
 610 nual Sea Level Co-Variability Between the Northeast and Southeast Coasts  
 611 of the United States? *Journal of Geophysical Research: Oceans*, *129*(1),  
 612 e2023JC019873. doi: 10.1029/2023JC019873
- 613 Wang, O., Lee, T., Piecuch, C. G., Fukumori, I., Fenty, I., Frederikse, T., ... Zhang,  
 614 H. (2022, June). Local and Remote Forcing of Interannual Sea-Level Vari-  
 615 ability at Nantucket Island. *Journal of Geophysical Research: Oceans*, *127*(6),  
 616 e2021JC018275. doi: 10.1029/2021JC018275
- 617 Wise, A., Hughes, C. W., & Polton, J. A. (2018, December). Bathymetric In-  
 618 fluence on the Coastal Sea Level Response to Ocean Gyres at Western  
 619 Boundaries. *Journal of Physical Oceanography*, *48*(12), 2949–2964. doi:  
 620 10.1175/JPO-D-18-0007.1
- 621 Woodworth, P. L., Maqueda, M. A. M., Roussenov, V. M., Williams, R. G., &  
 622 Hughes, C. W. (2014, December). Mean sea-level variability along the north-  
 623 east American Atlantic coast and the roles of the wind and the overturning  
 624 circulation. *Journal of Geophysical Research: Oceans*, *119*(12), 8916–8935. doi:  
 625 10.1002/2014JC010520
- 626 Woodworth, P. L., Morales Maqueda, M. A., Gehrels, W. R., Roussenov, V. M.,  
 627 Williams, R. G., & Hughes, C. W. (2017, October). Variations in the dif-  
 628 ference between mean sea level measured either side of Cape Hatteras and  
 629 their relation to the North Atlantic Oscillation. *Climate Dynamics*, *49*(7-8),  
 630 2451–2469. doi: 10.1007/s00382-016-3464-1
- 631 Yin, J., & Goddard, P. B. (2013). Oceanic control of sea level rise patterns along  
 632 the East Coast of the United States. *Geophysical Research Letters*, *40*(20),  
 633 5514–5520. doi: 10.1002/2013GL057992
- 634 Yin, J., Schlesinger, M. E., & Stouffer, R. J. (2009, April). Model projections of  
 635 rapid sea-level rise on the northeast coast of the United States. *Nature Geo-  
 636 science*, *2*(4), 262–266. doi: 10.1038/ngeo462
- 637 Zhu, Y., Han, W., & Alexander, M. A. (2023). Nonstationary Roles of Regional  
 638 Forcings in Driving Low-Frequency Sea Level Variability Along the U.S. East  
 639 Coast Since the 1950s. *Geophysical Research Letters*, *50*(15), e2023GL104191.  
 640 doi: 10.1029/2023GL104191